THE JOURNAL OF NAVIGATION (2016), **69**, 1–23.
doi:10.1017/S0373463315000570

Reconstructing the Malaysian 370 Flight Trajectory by Optimal Search

Octavian Thor Pleter, Cristian Emil Constantinescu and Barna Istvan Jakab

(*University Politehnica of Bucharest, 060042 Bucharest, Romania*)
(E-mail: otp@brainbond.ro)

In the aftermath of the disappearance of the Malaysian 370 (MH370) flight in March 2014, new positioning methods were employed to establish the search area. In the absence of all other positioning technologies (Transponder, Radio communications, Radar), these innovative methods are based on the handshake signals between an INMARSAT satellite and the satellite transceiver on board the aircraft. The log of these signals was made public in order for the scientific community to engage in solving the mystery of the MH370 trajectory. The log indicates the delay between the interrogation and response signals, as well as the relative velocity indications, based on the shift of the carrier frequency due to the Doppler-Fizeau effect. This paper puts forward an original, independent and accurate positioning method and allows the calculation of the MH370 trajectory considering the wind vector field that day, the accurate satellite orbit and an accurate model of the Earth (the WGS-84 ellipsoid). The results were compared to other results published, indicating a different final position of the aircraft from the locations of the published search area.

KEYWORDS

1. MH370. 2. Trajectory. 3. Search and Rescue (SAR).

Submitted: 13 January 2015. Accepted: 1 July 2015. First published online: 30 July 2015.

1. INTRODUCTION. On 8 March 2014, the flight Malaysian 370 from Kuala Lumpur to Beijing disappeared without any trace. The aircraft was a Boeing 777-200ER (777-2H6ER, ICAO type designator B772) with the registration 9M-MRO. After 32 minutes of flight preparation, the aircraft took off and flew normally for 49 minutes. After the crucial point of IGARI at the border between Malaysian and Vietnamese airspace, the aircraft made abnormal manoeuvres for 1 hour and 17 minutes (turns, climbs, descents) then settled for a long range flight of 5 hours and 42 minutes. The total time flown abnormally was 7 hours, most probably until the fuel was exhausted. The long range en route flight of almost 6 hours was probably under automated guidance, very probably following a keyboard input flight plan changed earlier during the flight. Although all communication systems were shut down in a time window of 12 minutes (from 1709Z to 1721Z), the SATCOM satellite transponder continued to be functional and provided a number of very important clues

Table 1. MH370 Flight Phases.

From	To	Phase	Duration	No
2014 March 8 00:00:13 (1600Z)	00:32:13 (1632Z)	Flight preparation	32′ 0″	1
---	---	*Start of flight*	**32′**	
00:32:14 (1632Z)	00:40:38 (1641Z)	Push-back, start and taxi	8′ 26″	2
00:40:38 (1641Z)	01:01:16 (1701Z)	Take-off and climb	20′ 38″	3
01:01:16 (1701Z)	01:21:04 (1721Z)	En route to IGARI	19′ 48″	4
---	---	*End of normal flight / Start of abnormal manoeuvers under military surveillance*	**49′**	
01:21:04 (1721Z)	02:22:00 (1822Z)	Manoeuvers under military surveillance	1 h 0′ 56″	5
---	---	*End of abnormal manoeuvers / Start of unknown flight*	**1 h 1′**	
02:22:00 (1822Z)	02:38:00 (1838Z) ?	Unknown continuation of the flight, including a turn onto a new flight track	Max 16′	6
02:38:00 (1838Z) ?	08:19:29 (0019Z)	Unknown en route flight	Min 5 h 42′	7
08:19:29 (0019Z) ?	08:28:29 (0028Z) ?	Glide descent with both engines out due to fuel starvation, until crash	≈ 9′	8
---	---	*End of flight*	**6 h 07′**	

about flight MH370. This paper is the result of the original work of the authors, calculating all trajectories of the aircraft consistent with a single turn after loss of ground radar contact. Also, an optimisation cycle was used to calculate the most probable trajectories, which fit best on all the data known. The results are surprising, because they indicate a position where the flight could have ended, which is different from the past and the current search areas. Besides its scientific relevance, the authors hope that their work will prove useful in the future search operations.

2. MH370 FLIGHT FACTS. Malaysian Airlines 370 took off with 239 Persons On Board (POB) (227 passengers out of the capacity of 282 and 12 members of crew). The initial flight plan was from Kuala Lumpur International (KLIA) to Beijing Capital International Airport (ZBAA). The ETA (Estimated Time of Arrival at planned destination (UTC)) was 2230Z and ETE (Estimated Time En route (estimated duration of flight in hours and minutes)) was 05:49. The fuel load was 49,100 kg, enough for over eight hours of flight. The MH370 flight phases are described in Table 1. Table 2 provides a detailed sequence of known facts about the flight, including the seven relevant ping exchanges between the INMARSAT-3 Indian Ocean Region (IOR) satellite and the SATCOM transceiver, which allow the calculation of the flight trajectory. The key moments of the flight are defined in Table 3.

The signal delay is called BTO (Burst Timing Offset) and it is caused by the time the radio waves take to travel from the satellite ground station to the satellite to the aircraft and back. Based on this, the instantaneous distance between the satellite and the aircraft (range) may be calculated for each ping exchange. The calculations presented in this paper rely mainly on these BTOs.

The locus of the points within a certain range is a sphere with the centre in the satellite position, with the range as the radius. This sphere may be intersected with the surface parallel to the ellipsoid or the geoid, at an altitude above the geoid, which

Table 2. Sequence of Known Facts about MH370.

Time	Event of the Flight MH370	Reference
2014 March 8	INMARSAT I-3 IOR Log-On	Avionics Power Up
00:00:13 (1600Z)		
00:07:00 (1607Z)	First Air DATA-2 ACARS[1] message BFO 86–90 Hz BTO 14780–14900 μs	First ACARS
00:25:53 (1626Z)	"Delivery Malaysian Three Seven Zero good morning"	ATC Delivery contact
00:27:27 (1627Z)	"Ground Malaysian Three Seven Zero good morning Charlie One requesting push and start"	LUMPUR GND contact
00:29:00 (1629Z)	ACARS message BFO 98–100 Hz BTO 14920–14940 μs	
00:32:13 (1632Z)	"Malaysian Three Seven Zero request taxi"	
00:36:30 (1637Z)	"Tower Malaysian Three Seven Zero morning"	LUMPUR TWR contact
00:40:38 (1641Z)	TWR: "Three Seven Zero Three Two Right Cleared for take-off good night" MH370: "Three Two Right Cleared for take-off Malaysian Three Seven Zero thank you bye"	T/O clearance
00:41:43 (1642Z)	Take-Off RWY 32R KLIA	
00:42:05 (1642Z)	"Departure Malaysian Three Seven Zero"	LUMPUR APP contact
00:42:07 (1642Z)	Cleared to climb to FL180 Direct IGARI	
00:42:52 (1643Z)	Transferred from LUMPUR APP to LUMPUR RADAR	
00:46:51 (1647Z)	"Lumpur Control Malaysian Three Seven Zero"	LUMPUR ACC contact
00:46:51 (1647Z)	Cleared to climb to FL250	
00:50:06 (1650Z)	Cleared to climb to FL350	
00:55:00 (1655Z)	ACARS message BFO 155–156 Hz BTO 15200–15220 μs	
01:01:16 (1701Z)	Pilot reports maintaining FL350 (unnecessary, unsolicited) HDG 025 GS 471 kts	Strange human action
01:07:49 (1708Z)	Last Air DATA-2 ACARS message BFO 131 Hz BTO 15620 μs	Last ACARS
01:07:55 (1708Z)	Pilot reports maintaining FL350 (unnecessary, unsolicited, repeated)	Strange human action
01:09:00 (1709Z)	FMS flight plan changed from the keyboard	(unconfirmed)
01:19:24 (1719Z)	Transferred from LUMPUR RADAR[2] to HCM ATCC[3] on 120·9 MHz – Last transmission from cockpit: "Good Night Malaysian Three Seven Zero"	Last COM
01:21:04 (1721Z)	Fly over IGARI N06°55′15″ E103°34′43″ (as tracked by LUMPUR RADAR) FOB[4] for 8 hours of flight	Exit Malaysian airspace
01:21:13 (1721Z)	Transponder switched off or failed	Last XPDR[5]
01:22:00 (1722Z)	Turn Left HDG	PSR[6] data
01:30:00 (1730Z)	HCM ACC requests other aircraft to relay communications to MHA 370 – no answer	No COM
01:37:00 (1737Z)	Expected ACARS message not transmitted	No ACARS
	Climb to FL450	PSR data
	Descend to FL120 (or lower)	PSR data
02:03:42 (1804Z)	No response to Air DATA-2 ACARS - ACARS failed or has been switched off between 01:07:49 and 02:03:41	Proof of no ACARS
02:22:00 (1822Z)	200 NM NW of Pinang – Last Military Primary Radar contact	Last PSR contact
02:25:28 (1825Z)	Ping Log-On request from aircraft BFO 142 Hz BTO 17120 μs	
02:25:34 (1825Z)	Ping handshake BFO 273 Hz BTO 51700 μs	
02:27:04 (1827Z)	Ping handshake BFO 175–176 Hz BTO 12560–12520 μs	
02:28:06 (1828Z)	Ping handshake BFO 144 Hz BTO 12500 μs	
02:28:15 (1828Z)	Ping handshake BFO 143 Hz BTO 12480 μs	

Continued

Table 2. (*Continued*)

Time	Event of the Flight MH370	Reference
02:39:53 (1840Z)	Ground initiated Air Telephony call	
02:40:56 (1841Z)	No answer – Ping handshake BFO 88–90 Hz	Strange human action
02:41:00 (1841Z)	ACC Subang notifies about losing the flight	Aircraft on a new track
03:41:03 (1941Z)	Ping handshake BFO 111 Hz BTO 11500 μs	
04:41:05 (2041Z)	Ping handshake BFO 141 Hz BTO 11740 μs	
05:30:00 (2130Z)	Search and Rescue (SAR) operation activated by Kuala Lumpur Rescue Coordination Centre (KL RCC)	
05:41:27 (2141Z)	Ping handshake BFO 168 Hz BTO 12780 μs	
06:41:22 (2241Z)	Ping handshake BFO 204 Hz BTO 14540 μs	
07:13:58 (2314Z)	Ground initiated Air Telephony call	Last Telephony Call[7]
07:15:02 (2315Z)	No answer – Ping handshake BFO 216–219 Hz	
08:11:00 (0011Z)	Ping handshake BFO 252 Hz BTO 18040 μs	Last complete Ping
08:19:29 (0019Z)	Last incomplete ping requested by user BFO 182 Hz BTO 23000 μs	Last incomplete Ping / both engines out
08:30:00 (0030Z)	Flight time limit based on FOB at FL310 or above at normal cruise airspeed $TAS = 470$ kts	
09:10:00 (0110Z)	Expected Ping handshake did not arrive	Proof of avionics out

[1] ACARS: Aircraft Communications Addressing and Reporting System, automated bidirectional system for technical and operational messages between aircraft and a ground communication network or a satellite communication network
[2] ACC Subang, Malaysia
[3] ACC Ho Chi Mingh, Vietnam
[4] FOB: Fuel on Board
[5] XPRD: Secondary Surveillance Transponder
[6] PSR: Primary Surveillance Radar (military)
[7] Not answered, but the subsequent ping proved aircraft to be in operational status.

Table 3. Key moments of the MH370 flight.

Malaysian Time	UTC	Identifier	Description
00:00:13	1600Z	t_L	Avionics power up and satellite **L**og on
00:41:43	1642Z	t_T	**T**ake-Off RWY 32R KLIA
01:07:49	1708Z	t_A	Last Air DATA-2 **A**CARS message
01:19:24	1719Z	t_C	Last **C**OM "Good Night Malaysian Three Seven Zero"
01:21:04	1721Z	t_X	Last **X**PDR fly over IGARI N06°55′15″ E103°34′43″
02:22:00	1822Z	t_M	Last **M**ilitary PSR contact 200 NM NW of Pinang
02:25:28	1825Z	t_1	**1**st complete satellite ping considered in the literature
$t_M + TTT$	$t_M + TTT$	t_S	**S**tart turn on a new track
03:41:03	1941Z	t_2	**2**nd complete satellite ping, the first on the new track
04:41:05	2041Z	t_3	**3**rd complete satellite ping, the 2nd on the new track
05:41:27	2141Z	t_4	**4**th complete satellite ping, the third on the new track
06:41:22	2241Z	t_5	**5**th complete satellite ping, the fourth on the new track
08:11:00	0011Z	t_6	**6**th complete satellite ping, the fifth on the new track
08:19:29	0019Z	$t_7 = t_G$	7th incomplete user request ping – **E**nd of powered flight, start glide with both engines out
$t_G + TGE$	$t_G + TGE$	t_E	End of flight

corresponds with the presumed flight level of the aircraft. This is in fact the isobaric surface for level flight, corresponding to the local meteorological data. The intersection yields a curve very close to a circle. At the given moment of the ping, the position of the aircraft is somewhere on that quasi-circle.

The shift in carrier frequency is called BFO (Burst Frequency Offset). It is caused by the Doppler-Fizeau effect due to the relative speed between the aircraft and the satellite. In the calculations below, the BFO values were not used, and this is a major difference between this method and other methods used until now and known to the authors (Ashton et al., 2014; Hradecky, 2014). The reason for avoiding the use of BFO values is that the problem of relative speed is geometrically ill conditioned in this case, especially in the first half of the flight.

3. CALCULATION OF QUASI-CIRCLES. This paper models the Earth as the WGS-84 ellipsoid. The ranges define quasi-circles at the intersection between the isobaric surface that the aircraft levels on, and the sphere with the centre in the satellite antenna position and the BTO-based range as the radius.

The INMARSAT-3 satellites are five satellites in 36,000 km high geostationary orbit (N0°), as follows: AOR-W at a longitude of W54°, AOR-E at W15·5°, I-3 at 25°E, IOR (the satellite used by MH370) at E64·5°, and POR at E178°. INMARSAT-3 IOR has an orbit inclined at 1·66°. This inclination gives a wobble movement with a period of T = 24 hours. The actual orbital altitude of IOR at t_6 was: 35,794 km, as compared to the target of 35,786 km Above Mean Sea Level (AMSL). Although geostationary, the actual position of the IOR satellite moved slightly during the MH370 flight.

In the Earth-Centred-Earth-Fixed (ECEF) frame, the system of equations used to calculate the seven quasi-circles (see Figure 8) are the WGS-84 rotation ellipsoid equations and the satellite-centred sphere equations:

$$n_\varphi = \frac{6378136{\cdot}6}{\sqrt{1 - e_2 \times (\sin\varphi)^2}} \tag{1}$$

$$\begin{cases} x = (n_\varphi + H)\cos\varphi\cos\lambda \\ y = (n_\varphi + H)\cos\varphi\sin\lambda \\ z = n_\varphi(1 - e_2) + H\sin\varphi \end{cases} \tag{2}$$

$$\sqrt{(x - x_{SAT})^2 + (y - y_{SAT})^2 + (z - z_{SAT})^2} - Range_{satellite\ to\ aircraft} = 0 \tag{3}$$

From (Ashton et al., 2014):

$$Range_{satellite\ to\ aircraft} = \frac{1}{2}c \cdot (BTO - bias) - Range_{satellite\ to\ Perth\ GES} \tag{4}$$

$$bias = -495679\ \mu s \tag{5}$$

The Equations (2) in x, y, z are substituted in Equation (3), providing a way to calculate longitude λ as a function of latitude φ. The seven quasi-circles correspond to the seven pings, illustrated in Figure 8, which occurred at the times t_1 to t_7 (see Table 3). However, the first complete satellite ping considered in the literature was not used in this paper, because the initialisation of the problem is uncertain, so less weight should be given to the starting point. Consequently, the work presented in this paper relies on the last six quasi-circles only. As a confirmation of this selection of quasi-circles, the contribution of the six pings to the total inconsistency of the trajectory is well balanced. The individual contribution of the first ping to the total inconsistency would have been disproportionately larger than the contributions of the other pings.

4. SOLVING TRAJECTORY EQUATIONS. The authors independently calculated the MH370 trajectory based on the following data:

1. Flight trajectory until the last known position P_18_22 as recorded by the military primary radars (N 6° 36′ 15″ E 96° 33′ 14″) (Malaysian Gov., 2014; Hradecky, 2014).
2. The set of recorded INMARSAT (INMARSAT, 2014) satellite pings (signal handshake delays and carrier frequency drift) (Malaysian Gov., 2014, Hradecky, 2014).
3. The wind vector field, isobaric surface height and air temperature in the wider area at the moment of the flight, retrieved from the National Oceanic and Atmospheric Administration (NOAA) 2014). Interpolations in time, position, and flight levels were used for the best local current estimate of the wind velocity and the air temperature.
4. The Boeing 777-200ER flight performance and systems (Boeing, 1992a). A Boeing 777-200ER flight simulator based on a dynamic model was developed by the authors (Section 5).
5. The Boeing 777-200ER FMS (Flight Management System) specifications (Bulfer and Gifford, 1999).
6. The WGS-84 ellipsoid shape approximation of the Earth.
7. The INMARSAT-3 IOR satellite orbital data (Malaysian Gov., 2014).

The unknowns of this problem and the space of solutions are considered in the following subsections (see Figure 1).

4.1. *The Time to Turn Unknown (TTT).* It was assumed that the flight continued straight for a while (on the track of 291° true) from the moment it vanished from the military primary radars (t_M or P_18_22). The duration of this straight segment *TTT* (Time To Turn) is one of the unknowns of the problem. *TTT* search domain was initially considered 0–50 minutes, then reduced to 5–16·75 minutes, based on the following:

- In numerical search trials, for *TTT* over 17 minutes, the breakdown of the quadratic error (ε) on the six quasi-circles starts to show an abnormal error increase for the first two quasi-circles;
- In both the uncorrected (Hradecky, 2014), and the corrected *BFO* diagram (Ashton et al., 2014), the turn is marked by a significant drop in the frequency due to the Doppler-Fizeau effect between the moments 1820Z and 1830Z, i.e. in an 11 minutes time interval;
- The dynamic model simulation presented further provides an additional validation for the upper limitation of this time to 16·75 minutes; if the flight continued on the initial track for 17 minutes or more, the optimised trajectory solutions (*TK*, *FL* and *M*) would largely disagree with the dynamic simulation (the fuel would have been exhausted before the last complete ping due to the required thrust settings resulting from *FL* and *M*);
- No consistent solution emerged for *TTT* shorter than 5 minutes.

After *TTT*, a coordinated turn was simulated, using a dynamic model Boeing 777-200ER simulator (see Section 5). The search step was one minute, refined down to five seconds for the promising domains.

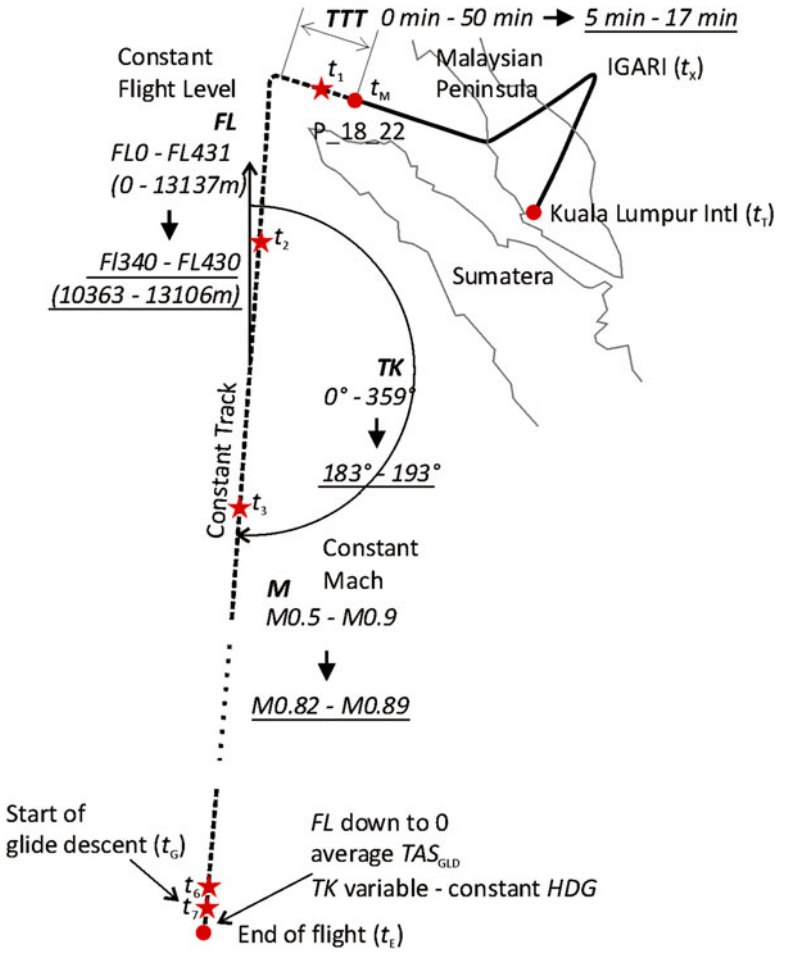

Figure 1. MH370 trajectory problem unknowns: *TTT*, *TK*, *FL*, and *M*.

This paper is based on the assumption that a single turn was made at the beginning of a long constant track segment. The *BFO* analysis (Figure 9 from Ashton et al., 2014) is consistent with a major turn between certain time moments: 1820Z and1830Z. After that turn, the *BFO* diagram indicates a linear variation of the Doppler-Fizeau frequency shift, i.e. no other turns. A notable fact is that one 360° turn at high *M* would typically last for 11·5 minutes, and the time window in the diagram is just too small for multiple turns concentrated at the beginning of the long constant track segment. On the other hand, multiple turns sparsely distributed over the entire voyage seem impossible given the same *BFO* diagram, because at each ping there is approximately the same *BFO*, the timing between pings is not always predictable (there are phone calls from the ground which spoil the one hour default time interval), and this is consistent with the hypothesis of an approximately constant ground speed vector. Another reason for the single turn assumption is the simplicity and the timing of the FMS programming. The programming of each additional turn into the FMS

should have been based on *ad hoc* navigation points entered individually as *LAT-LONG*. Attempting such a scenario on a flight simulator indicated a significant duration of the operation, not consistent with the existing time window in this case.

One additional rationale of the single turn hypothesis comes from the speculation on the goal of the person who did program the FMS as such. The goal of this action could have been to hide evidence in a place as remote as possible. The choice of track coincides with such a strategy, to end the flight as far as possible from any populated or frequented area. Programming multiple turns into the FMS would have been pointless and detrimental to the goal of flying as far as possible. This is speculative, but it only supplements all the other non-speculative grounds of the single turn assumption.

4.2. *The Track Unknown (TK).* After *TTT* minutes, the aircraft took a turn to an unknown track *TK* (presumed constant), and from that moment it kept that track for the entire duration of the flight, until both engines became fuel starved. This is consistent with the variation of the frequency shift due to the Doppler-Fizeau effect on the carrier (the seven *BFO*s). Initially, all possible tracks were considered, (0°–359°), but a refined search was performed in the promising range of 170°–200° (the Southern range), and finally in the range 183°–193°, because all solutions obviously proved to be concentrated within these limits. The search step was 1°. The next best promising interval lays in the Northern range (around 336°) was not considered in the refined search for the following reasons:

- The Northern tracks lead to inconsistencies at least three times larger than the Southern tracks;
- In both the uncorrected (Hradecky, 2014), and the corrected BFO diagram (Ashton et al., 2014), the Southern variant matches very well the expected set of *BFO*s, in contrast with the Northern variant.

This constant track phase of the flight (Phase 7 in Table 1) was probably flown under automated guidance, until the airplane became fuel starved, glided down and crashed. Other authors considered a constant heading for the flight. Although the Boeing 777 autopilot has a function to maintain a constant heading (HDG HOLD on the Mode Control Panel–Boeing, 1992b), it is unlikely that this flight was not under FMS guidance (LNAV mode), and in this case *HDG* changes automatically to compensate for the crosswind. Thus, it is logical to assume a constant track flight (loxodrome or rhumb line) instead of a constant heading flight. A third hypothesis concerns a "DIRECT TO" a distant point flight, which would force navigation along the great circle (orthodrome). However, in the particular case of MH370, the difference between the orthodrome and the loxodrome routes is insignificant, and thus the constant track route covers both scenarios. A fourth hypothesis is a flight with the autopilot engaged in the "TRK HOLD" mode (constant track). This is also covered by the assumption made in this paper.

4.3. *The Flight Level Unknown (FL).* The flight level (*FL*) of the cruise flight is presumed constant. Initially, all possible flight levels from 0 ft to 43,100 ft were considered. The problem is not very sensitive to the geometric *FL* variable, except for the way the speed was formalised (see the Mach number below), where the temperature matters to a large extent. Also, the wind velocity changes from one level to the other, leading to significant differences between the flight levels. Very soon in the initial phase of the

Table 4. The subspace of solutions for refined search.

Unknown	Significance	Units	Min	Max	Step	Layers
TTT	Time to turn	Minutes	5	16·75	0·25	48
TK	Track	°	183	193	1	11
FL	Flight level	×100 feet	340	430	10	10
M	Mach number	–	0·82	0·89	0·01	8
Total						42,240

optimisation process, it became obvious that flight levels below FL340 were impossible, for two reasons:

- The inconsistency of these solutions is unacceptably high;
- The dynamic model simulation indicated that achieving a time of flight until the last half ping (t_7) would require a lower density of air.

The fine phase of the optimisation was performed on a search range between FL340 (34,000 ft) and FL430 (43,000 ft), with a step of 1,000 ft.

The authors found no grounds to consider a variable flight level and Mach number along the cruise. Flying under FMS guidance would require a constant flight level selected for cruise, and the same value input in the altitude selector on the Mode Control Panel (Boeing, 1992b; Bulfer and Gifford, 1999).

4.4. *The Mach Number Unknown (M).* The Mach number (*M*) is presumed constant. The initial search domain was between M0·65 and M0·9, but the envelope was correlated with *FL* following the flight performance of the aircraft type. The reason for choosing Mach instead of True Airspeed (*TAS*), Indicated Airspeed (*IAS*), or Ground Speed (*GS*) is related to the operational logic of the Flight Management System, Auto-Pilot and Auto-Throttle System on board the Boeing 777 aircraft. There is a slight difference in the final result between maintaining a constant *M* and a constant *TAS*, and this comes from the outside temperature variations. The height of the isobaric surfaces, air temperatures and the wind velocity vectors along the route were taken from the NOAA archives (NOAA, 2014), as per the date and the hour of the flight. Interpolation in time, interpolation in the vertical profile of the wind vector field and interpolation in position data provide the best approximations of the real meteorological parameters. For the later stages of the optimisation, the Mach search range was reduced to M0·82–M0·89. Whereas the maximum Mach number was delivering many consistent solutions, the lower speeds proved to be constantly inconsistent and were discarded. The search step for the Mach number was 0·01.

4.5. *Assumptions for the Last Segment of the Flight.* The last incomplete user requested ping at t_7 is considered to mark the end of the powered flight, and the start of a powerless glide. The accurate simulation of the flight using a dynamic model (see Section 5) confirms this hypothesis, with a low error margin between the timing in the simulator and the timing of the ping signals (see Table 7).

The last segment of the flight was a glide with both engines out due to fuel starvation (Pleter and Constantinescu, 2014).

4.6. *Trajectory Equations.* Given the above considerations, the space of solutions was reduced from 34,056,000 initial possible solutions down to 42,240 possible trajectories, as summarised in Table 4 and illustrated in Figure 1 by underlined text.

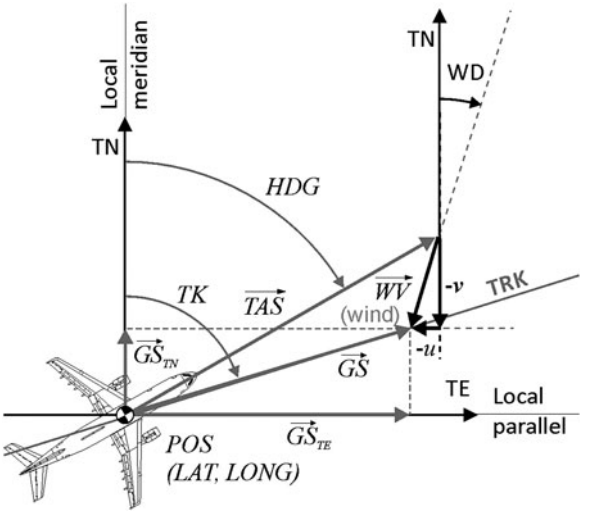

Figure 2. Local wind triangle solved at each time step in the course of flight simulation.

Considering the True North (u) and the True East (v) components of the local horizontal wind velocity vector retrieved from the NOAA records, the speed triangle system of trigonometric equations is the following (see Figure 2):

$$\begin{cases} TAS \cdot \cos HDG + v = GS \cdot \cos TK \\ TAS \cdot \sin HDG + u = GS \cdot \sin TK \end{cases} \tag{6}$$

The solution of the system is the following:

$$HDG = \mp 2 \tan^{-1}\left(\frac{\pm TAS \cdot \cos TK + \sqrt{TAS^2 - (u \cdot \cos TK - v \cdot \sin TK)^2}}{u \cdot \cos TK + (TAS - v) \cdot \sin TK}\right) \tag{7}$$

$$GS = v \cdot \cos TK + u \cdot \sin TK \mp \sqrt{TAS^2 - (u \cdot \cos TK - v \cdot \sin TK)^2} \tag{8}$$

The system of six equations that result from the data (the time delays BTO of the six relevant pings) is over determined, and it was solved so as to minimise the quadratic sum of errors, which was considered as the inconsistency of the solution (E). The inconsistency was calculated and used as an optimisation criterion to refine the search to the most plausible solution:

$$\varepsilon = \sqrt{\sum_1^6 d_i^2} = min \tag{9}$$

Each of the six errors d_i is the distance between the aircraft at the moment of each of the six pings, and the closest point belonging to the respective quasi-circle.

The flight was simulated using a Runge-Kutta IV method with a time step of 10 seconds, integrating the local speed triangle (Figure 2) and the dynamic flight

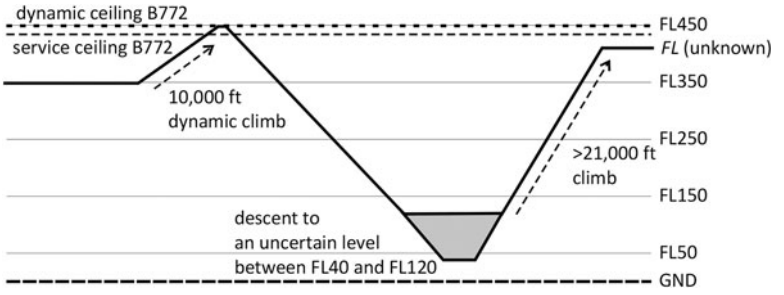

Figure 3. The flight profile of the MH370 under military primary radar surveillance.

simulator equations. At the moments of the pings, the position resulting from the simulation was compared to the position resulting from the radio transmission by calculating the distance d_i between the two. The quadratic sum of distances d_i was minimised using a complete search optimisation method. All calculations were done by a MATLAB application written by the authors.

The wind velocity and air temperature were retrieved from the NOAA world weather database (NOAA, 2014), with a granulation of 0·5° of latitude and longitude. Linear interpolation of latitude and longitude was used between the nodes. Vertically, the data are presented for the following isobaric surfaces: 10, 20, 30, 50, 70, 100, 150, 200, 250, 300, 350, 400, 450, 500, 550, 600, 650, 700, 750, 800, 850, 900, 925, 950, 975, and 1000 mbar. These isobars are converted into flight levels using the ISA model, and linear interpolation was used between the isobaric surfaces.

5. THE DYNAMIC MODEL FLIGHT SIMULATOR. For the purpose of this research, a Boeing 777-200ER flight simulator was developed. The simulator is based on a dynamic model i.e. considers the mass of the aircraft and calculates the fuel flow at each time step. The simulator served three separate goals:

- To integrate the flight trajectory, the current mass of the aircraft, and the fuel consumption. By comparing the fuel consumption to the known fuel on board in the first stage of the flight, one can determine the approximate moment of fuel exhaust. This is compared to t_G, which results from optimisation (see Table 7).
- To calculate the fuel consumption of a dynamic climb to FL450, a descent to FL120 or below, and a climb back to an unknown cruise *FL* (Figure 3). These manoeuvres were recorded by the military primary surveillance radars, so the exact levels or details of the manoeuvres are not known. Instead of a simulator based on a time step integration, the authors used a method based on energy and aircraft climb / descent efficiency to calculate the fuel consumed by it.
- To simulate the final glide descent portion, since the start of glide descent (t_G) until crash (t_E).

Table 5. Aerodynamic Coefficients for Boeing 777 (Pereira, 2011).

$C_{L\alpha}$	C_{D0}	α_{CL0}	K_2
5·1	0·013	−2·8°	0·047

The equations of the simulator are the following:

$$TAS = M \cdot a \tag{10}$$

$$C_L = C_{L\alpha} \cdot (\alpha - \alpha_{CL0}) \tag{11}$$

$$C_D = C_{D0} + K_2 \cdot C_L^2 \tag{12}$$

$$L = \frac{\rho_0}{2} \cdot TAS^2 \cdot S \cdot C_L \tag{13}$$

$$D = \frac{\rho_0}{2} \cdot TAS^2 \cdot S \cdot C_D \tag{14}$$

$$T = \frac{D}{\cos(\alpha + \tau)} \tag{15}$$

$$T \cdot \sin(\alpha + \tau) + L = m \cdot g \cdot \cos(\phi) \tag{16}$$

The coefficients used for Boeing 777 are as presented in Table 5.

Simulation of the fuel consumption between the last ACARS message and last military primary radar contact was done with the following equations:

$$FF_{avg} \cdot (t_M - t_A) + FC_{\Delta E} = FC_{total} \tag{17}$$

$$FC_{\Delta E} = \frac{\Delta E_p + \Delta E_c}{s \cdot eff} \tag{18}$$

The efficiency *eff* of the engines was calibrated based on the FOB at engine start and FOB at the moment of the last ACARS message (A). The taxi fuel consumption was calculated using the following formula:

$$\frac{f}{\sqrt{T_{amb}}} = a_{taxi} + b_{taxi} \cdot t_{taxi} + c_{taxi} \cdot na \tag{19}$$

where $a_{taxi} = -0{\cdot}1223$ $b_{taxi} = 0{\cdot}0335$ $c_{taxi} = 0{\cdot}1385$ are the coefficients for a Boeing 777, na is the number of accelerations during taxi (it is considered to be at least two) and the ambient temperature in Kuala Lumpur in March during night was assumed to be $T_{amb} = 297{\cdot}15\ K$ (Khadilkar, 2011). The taxi fuel consumption which results from the above equation is $f = 457{\cdot}8\ kg$. The remaining FOB at take-off is 49100–457·8 = 48612 kg. Knowing the FOB broadcast by the last ACARS message (43,800 kg) and considering an average fuel flow of $FF_{avg} = 6406\ kg/h$ and the specific energy of Jet A-1, $s = 43{\cdot}02\ MJ/kg$, the resultant efficiency of the engines is 32·32%. In this case, both the kinematic and the potential energy of the aircraft change. Using the calibrated engine efficiency, the resulting fuel consumption between the last ACARS message (A) and last military primary surveillance radar contact (M) is approximately 10,000 kg, depending on the FL to which the aircraft is considered to have climbed for the long cruise flight towards the south. For example, if the aircraft climbs to FL390, the calculated fuel consumption for the

Table 6. Equation (20) Coefficients.

$p_{0,0}$	$p_{1,0}$	$p_{0,1}$
31·47	0·004923	0·01895

last ACARS – last primary radar contact segment is $FC_{total} = 10065{\cdot}3\ kg$. In this case only the change in potential energy is considered (calculated with an average mass) and only at the climb regions. It is supposed that the fuel economy during the descending portions of the flight is balanced by the higher consumption in the dense air.

Simulation of fuel flow during the long cruise flight is based on Boeing (1992a) and Filippone (2006). Using the calculated thrust and the mass of the aircraft, the following polynomial equation was defined (coefficients are given in Table 6):

$$FF/ENG = p_{0,0} + p_{1,0} \cdot m + p_{0,1} \cdot T \tag{20}$$

Simulation of the final glide descent with both engines out in the time interval *TGD* presumed 9 minutes is presented in Pleter and Constantinescu (2014).

During the cruise flight, *TK* is kept constant by small turns, which compensate for crosswind. However, in the glide descent region, the simulation keeps a constant *HDG* instead of *TK*, and these turns are no longer performed, as illustrated in the inset in Figure 8. This is consistent with the expected behaviour of the automated systems. By keeping a constant *HDG*, the local crosswind slightly drifted the aircraft during the gliding descent.

6. ANALYSIS OF RESULTS. The multimodal optimisation using ε as a criterion (inconsistency to be minimised) yields the most probable trajectories and the most probable values of the unknowns *TTT*, *TK*, and *M*. The unknown *FL* is considered a parameter, because the problem is not sensitive with respect to the geometric *FL*. Just two *TK* ranges came out to be consistent: the Southern track around 190° (true) and the Northern track of around 336°. The Southern track fits better (a very low inconsistency, 38 solutions between 16 and 25 km), whereas the Northern track does not fit so well (zero solutions under 30 km).

The multimodal optimisation yields the set of all solutions with a certain minimum probability instead of a single most probable solution. Given the nature of the problem and the scarcity of data coming from a unique source, this approach adds more value than the initial search done by the same authors for the most probable trajectory (Pleter and Constantinescu, 2014). Thus all trajectories with an overall inconsistency lower than 25 km were considered as potential solutions, and they are represented in Tables 7 and 8, and in Figures 4 to 6. The threshold of 25 km is remarkably low as compared to the total length of the trajectory (almost 6,000 km). There are 38 consistent solutions (with $\varepsilon \leqslant 25$ km), and they are analysed in Table 7 and in the subsequent Figures. In Figure 4 all the 38 consistent solutions were represented as cylinders. The diameter of the cylinder is the inverse function of the inconsistency, i.e. consistency $(1/\varepsilon)$.

The most consistent solutions presented in Table 7 have a remarkably low inconsistency, of $\varepsilon < 17$ km. Column "Fuel error" in Table 7 (second part) compares the top of descent (t_G) calculated with the optimisation method based on the satellite pings and

Table 7. Consistent MH370 trajectory solutions and the corresponding positions of the end of flight (E) – solutions in yellow are confirmed by the available fuel criterion, with a fuel error ≤ 1%.

Solution	ε (km)	TTT (min)	TK (°)	M (-)	FL (ft)	LAT_2 (°)	$LONG_2$ (°)	GS_2 (kts)	LAT_3 (°)	$LONG_3$ (°)	GS_3 (kts)	LAT_4 (°)	$LONG_4$ (°)	GS_4 (kts)	LAT_5 (°)	$LONG_5$ (°)	GS_5 (kts)
1	24·9	7:10	191	0·87	38,000	−2·58	93·51	501·9	−10·79	91·88	508·1	−19·13	90·22	493·5	−27·00	88·48	469·8
2	23·3	7:25	191	0·86	36,000	−2·59	93·49	503·3	−10·80	91·86	506·5	−19·14	90·19	499·6	−27·02	88·46	470·2
3	22·3	7:40	191	0·85	34,000	−2·61	93·47	505·1	−10·81	91·83	505·1	−19·16	90·17	505·9	−27·06	88·43	471·1
4	24·3	8:00	190	0·88	42,000	−2·25	93·61	492·6	−10·33	92·15	499·0	−18·57	90·65	493·9	−26·46	89·10	468·3
5	24·3	8:05	190	0·87	40,000	−2·28	93·61	494·2	−10·39	92·15	500·9	−18·65	90·65	490·9	−26·50	89·10	465·7
6	19·8	8:40	190	0·87	39,000	−2·24	93·54	498·3	−10·42	92·06	505·2	−18·75	90·56	491·7	−26·61	88·99	467·5
7	17·9	8:50	190	0·86	37,000	−2·27	93·52	499·2	−10·45	92·05	503·7	−18·77	90·55	495·4	−26·64	88·98	467·6
8	16·4	9:05	190	0·85	35,000	−2·28	93·50	500·4	−10·46	92·02	501·7	−18·78	90·52	500·9	−26·67	88·95	468·4
9	21·5	9:30	189	0·88	43,000	−1·92	93·63	489·6	−9·95	92·31	495·0	−18·14	90·97	494·7	−26·06	89·59	467·8
10	21·5	9:35	189	0·87	41,000	−1·94	93·63	490·8	−10·01	92·32	496·6	−18·23	90·98	492·6	−26·09	89·59	465·1
11	23·9	10:05	189	0·88	42,000	−1·88	93·56	493·4	−9·98	92·24	498·9	−18·23	90·89	496·3	−26·17	89·49	469·3
12	17·6	10:10	189	0·87	40,000	−1·88	93·54	494·7	−10·02	92·22	500·8	−18·30	90·88	494·0	−26·19	89·48	466·7
13	16·2	10:25	189	0·86	38,000	−1·91	93·53	495·9	−10·06	92·21	501·3	−18·36	90·87	493·8	−26·23	89·47	465·4
14	14·9	10:35	189	0·85	36,000	−1·94	93·52	496·3	−10·09	92·20	499·0	−18·38	90·85	497·3	−26·26	89·45	466·4
15	13·9	10:50	189	0·84	34,000	−1·96	93·49	497·2	−10·12	92·17	496·9	−18·40	90·82	501·1	−26·30	89·42	467·8
16	22·0	10:55	188	0·87	42,000	−1·64	93·66	487·4	−9·65	92·50	492·4	−17·82	91·31	491·9	−25·70	90·09	465·6
17	24·7	11:00	189	0·86	37,000	−1·88	93·45	499·2	−10·08	92·12	503·3	−18·42	90·77	498·0	−26·34	89·36	468·7
18	19·7	11:10	188	0·87	42,000	−1·59	93·63	487·6	−9·61	92·47	492·6	−17·77	91·29	492·0	−25·66	90·06	466·0
19	24·5	11:30	188	0·88	43,000	−1·55	93·57	490·2	−9·61	92·40	494·8	−17·81	91·21	495·3	−25·77	89·98	469·6
20	17·1	11:45	188	0·87	41,000	−1·55	93·55	491·4	−9·63	92·39	496·7	−17·86	91·20	494·6	−25·77	89·96	467·0
21	17·0	11:55	188	0·86	39,000	−1·57	93·55	492·8	−9·69	92·38	498·9	−17·96	91·19	493·5	−25·82	89·95	464·2
22	17·0	12:05	188	0·85	37,000	−1·60	93·53	493·0	−9·72	92·36	496·9	−17·98	91·18	495·1	−25·85	89·94	464·4
23	16·1	12:10	188	0·84	35,000	−1·63	93·51	493·3	−9·74	92·34	494·2	−17·99	91·15	497·6	−25·88	89·91	465·3
24	23·5	12:30	188	0·86	38,000	−1·53	93·46	496·1	−9·70	92·28	501·3	−18·02	91·09	496·7	−25·92	89·84	466·7

25	18·0	12:40	187	0·87	43,000	−1·25	93·63	484·4	−9·22	92·62	488·1	−17·33	91·59	489·2	−25·24	90·53	467·9
26	23·6	12:40	188	0·85	36,000	−1·55	93·43	496·2	−9·72	92·26	498·5	−18·03	91·07	499·1	−25·95	89·82	467·6
27	24·2	12:45	187	0·86	41,000	−1·28	93·63	485·5	−9·27	92·62	490·5	−17·42	91·60	489·7	−25·28	90·53	464·1
28	17·1	13:15	187	0·87	42,000	−1·21	93·56	488·2	−9·24	92·54	492·5	−17·42	91·50	492·4	−25·35	90·43	468·5
29	17·8	13:25	187	0·86	40,000	−1·23	93·55	489·4	−9·29	92·53	495·0	−17·51	91·50	492·7	−25·39	90·42	465·0
30	21·5	13:35	187	0·85	38,000	−1·26	93·54	490·1	−9·34	92·52	495·6	−17·58	91·49	493·0	−25·43	90·41	462·9
31	21·6	13:40	187	0·84	36,000	−1·30	93·52	489·9	−9·38	92·51	492·5	−17·60	91·48	493·7	−25·47	90·40	463·3
32	22·0	13:50	187	0·83	34,000	−1·34	93·50	490·2	−9·43	92·49	489·7	−17·63	91·45	494·9	−25·53	90·38	464·3
33	23·9	14:00	187	0·86	39,000	−1·20	93·47	493·2	−9·33	92·45	499·4	−17·61	91·41	495·4	−25·52	90·32	465·9
34	20·7	14:45	186	0·87	43,000	−0·86	93·55	485·0	−8·85	92·68	487·6	−16·97	91·80	489·3	−24·91	90·89	470·2
35	19·4	14:55	186	0·86	41,000	−0·89	93·54	485·9	−8·90	92·68	490·4	−17·05	91·80	490·6	−24·95	90·88	466·1
36	24·6	15:05	186	0·85	39,000	−0·92	93·54	487·2	−8·96	92·67	493·9	−17·16	91·80	491·9	−25·01	90·88	461·7
37	23·6	15:45	185	0·86	43,000	−0·59	93·62	478·9	−8·49	92·90	480·7	−16·51	92·17	484·5	−24·39	91·43	467·2
38	22·5	16:20	185	0·86	42,000	−0·56	93·54	482·4	−8·52	92·82	484·8	−16·61	92·09	487·8	−24·51	91·34	467·4

Solution	ε (km)	*TTT* (min)	*TK* (°)	*M* (–)	*FL* (ft)	LAT_6 (°)	$LONG_6$ (°)	GS_6 (kts)	LAT_7 (°)	$LONG_7$ (°)	GS_7 (kts)	LAT_E (°)	$LONG_E$ (°)	*Fuel Error* (%)	(sec)	ε* *w/o wind* (km
1	24·9	7:10	191	0·87	38,000	−38·57	85·64	478·4	−39·66	85·34	475·1	−40·42	85·14	−2·6%	−681	195·8
2	23·3	7:25	191	0·86	36,000	−38·54	85·63	479·0	−39·64	85·34	474·0	−40·40	85·14	−4·6%	−1186	174·3
3	22·3	7:40	191	0·85	34,000	−38·55	85·62	480·0	−39·64	85·34	473·2	−40·41	85·15	−7·2%	−1859	154·6
4	24·3	8:00	190	0·88	42,000	−38·09	86·52	477·5	−39·18	86·25	474·8	−39·94	86·07	1·0%	251	188·9
5	24·3	8:05	190	0·87	40,000	−38·02	86·53	475·4	−39·12	86·26	472·1	−39·88	86·08	−0·4%	−95	187·0
6	19·8	8:40	190	0·87	39,000	−38·17	86·41	476·8	−39·26	86·14	473·6	−40·02	85·96	−1·5%	−392	194·7
7	17·9	8:50	190	0·86	37,000	−38·14	86·41	476·5	−39·24	86·15	472·8	−40·00	85·97	−3·2%	−836	178·4
8	16·4	9:05	190	0·85	35,000	−38·14	86·40	477·0	−39·23	86·14	472·7	−40·00	85·97	−5·5%	−1418	163·5
9	21·5	9:30	189	0·88	43,000	−37·70	87·28	476·8	−38·80	87·04	474·3	−39·56	86·88	1·6%	424	190·1
10	21·5	9:35	189	0·87	41,000	−37·63	87·29	474·9	−38·73	87·05	471·6	−39·49	86·88	0·6%	151	186·7
11	23·9	10:05	189	0·88	42,000	−37·83	87·17	478·3	−38·94	86·93	475·4	−39·70	86·77	1·0%	253	200·8
12	17·6	10:10	189	0·87	40,000	−37·75	87·17	476·5	−38·85	86·93	472·8	−39·62	86·76	−0·4%	−95	263·9
13	16·2	10:25	189	0·86	38,000	−37·71	87·16	475·3	−38·81	86·93	471·1	−39·57	86·76	−2·1%	−533	181·0
14	14·9	10:35	189	0·85	36,000	−37·71	87·16	474·7	−38·80	86·93	470·8	−39·57	86·77	−4·0%	−1028	164·9

Continued

Table 7. (*Continued*)

Solution	ε (km)	*TTT* (min)	*TK* (°)	*M* (–)	*FL* (ft)	LAT_6 (°)	$LONG_6$ (°)	GS_6 (kts)	LAT_7 (°)	$LONG_7$ (°)	GS_7 (kts)	LAT_E (°)	$LONG_E$ (°)	*Fuel Error* (%)	(sec)	ε* *w/o wind* (km
15	13·9	10:50	189	0·84	34,000	−37·72	87·14	474·6	−38·82	86·92	470·9	−39·58	86·76	−6·5%	−1688	144·7
16	22·0	10:55	188	0·87	42,000	−37·25	88·05	473·9	−38·35	87·84	471·1	−39·11	87·70	1·4%	355	197·6
17	24·7	11:00	188	0·86	37,000	−37·88	87·05	477·2	−38·99	86·81	473·3	−39·75	86·65	−3·2%	−839	184·5
18	19·7	11:10	188	0·87	42,000	−37·21	88·03	474·1	−38·31	87·82	471·3	−39·07	87·68	1·4%	355	182·6
19	24·5	11:30	188	0·88	43,000	−37·44	87·92	477·5	−38·55	87·71	475·0	−39·31	87·58	1·7%	427	204·7
20	17·1	11:45	188	0·87	41,000	−37·34	87·92	475·8	−38·45	87·70	472·6	−39·21	87·56	0·6%	154	193·8
21	17·0	11:55	1E8	0·86	39,000	−37·28	87·91	474·4	−38·38	87·70	470·4	−39·15	87·56	−1·0%	−254	18E6
22	17·0	12·05	188	0·85	37,000	−37·27	87·91	473·2	−38·36	87·70	469·0	−39·13	87·56	−2·6%	−683	170·4
23	16·1	12:10	188	0·84	35,000	−37·28	87·89	472·3	−38·37	87·69	467·9	−39·13	87·55	−4·9%	−1256	155·8
24	23·5	12:30	188	0·86	38,000	−37·44	87·79	476·1	−38·54	87·58	472·1	−39·31	87·44	−2·1%	−533	189·6
25	18·0	12:40	187	0·87	43,000	−36·80	88·76	473·4	−37·90	88·58	470·5	−38·66	88·46	2·0%	517	184·7
26	23·6	12:40	188	0·85	36,000	−37·44	87·78	475·1	−38·54	87·58	471·0	−39·30	87·43	−4·0%	−1034	173·8
27	24·2	12:45	187	0·86	41,000	−36·73	88·76	471·6	−37·82	88·58	468·4	−38·59	88·46	1·0%	268	1810
28	17 1	13·15	187	0·87	42,000	−36·93	88·65	474 8	−38 03	88·47	472 0	−38 80	88·35	1·4%	358	194·7
29	17·8	13:25	187	0·86	40,000	−36·86	88·65	473·2	−37·96	88·47	469·9	−38·73	88·34	0·1%	34	185·4
30	21·5	13:35	187	0·85	38,000	−36·83	88·64	471·8	−37·92	88·46	467·9	−38·69	88·33	−1·5%	−386	174·3
31	21·6	13:40	187	0·84	36,000	−36·84	88·64	470·6	−37·93	88·46	465·8	−38·69	88·33	−3·4%	−869	158·3
32	22·0	13:50	187	0·83	34,000	−36·87	88·63	469·7	−37·96	88·45	464·0	−38·72	88·32	−5·9%	−1514	144·8
33	23·9	14:00	187	0·86	39,000	−37·01	88·54	474·9	−38·12	88·36	471·5	−38·88	88·23	−10%	−254	192·4
34	20·7	14:45	186	0·87	43,000	−36·51	89·37	474·6	−37·61	89·22	471·3	−38·37	89·12	2·0%	520	196·5
35	19·4	14:55	186	0·86	41,000	−36·44	89·37	472·5	−37·53	89·22	469·1	−38·30	89·11	1·0%	268	185·5
36	24·6	15:05	186	0·86	39,000	–3638	29·37	470·5	−37·48	89·21	467·1	−38·24	89·10	−0·5%	−116	177·7
37	23·6	15:45	185	0·86	43,000	−35·87	90·18	471·1	−36·97	90·05	466·7	−37·73	89·97	2·3%	604	185·9
38	22·5	16:20	185	0·86	42,000	−36·01	90·09	472·1	−37·11	89·96	467·9	−37·88	89·88	1·8%	461	186·8

Table 8. Flight level distribution of the consistent MH370 trajectory solutions.

FL	340	350	360	370	380	390	400	410	420	430
Number of solution $\varepsilon < 25$ km	3	2	4	3	4	4	3	4	6	5
Average ε	19·41	16·22	20·87	19·86	21·54	21·32	18·73	20·53	21·57	21·65
ε	***3*** 22	***8*** 16·36	***2*** 23·31	***7*** 17·94	***1*** 24·93	***6*** 19·83	***5*** 20·79	***10*** 21·49	***4*** 24·33	***9*** 21·46
	15 13·92	***23*** 16·08	***14*** 14·93	***17*** 24·66	***13*** 16·24	***21*** 16·99	***12*** 17·64	***20*** 17·05	***11*** 23·88	***19*** 24·49
	32 22·01		***26*** 23·64	***22*** 16·98	***24*** 23·45	***33*** 23·88	***29*** 17·75	***27*** 24·18	***16*** 22·03	***25*** 18·01
			31 21·61		***30*** 21·54	***36*** 24·58		***35*** 19·41	***18*** 19·65	***34*** 20·67
									28 17·08	***37*** 23·63
									38 22·47	

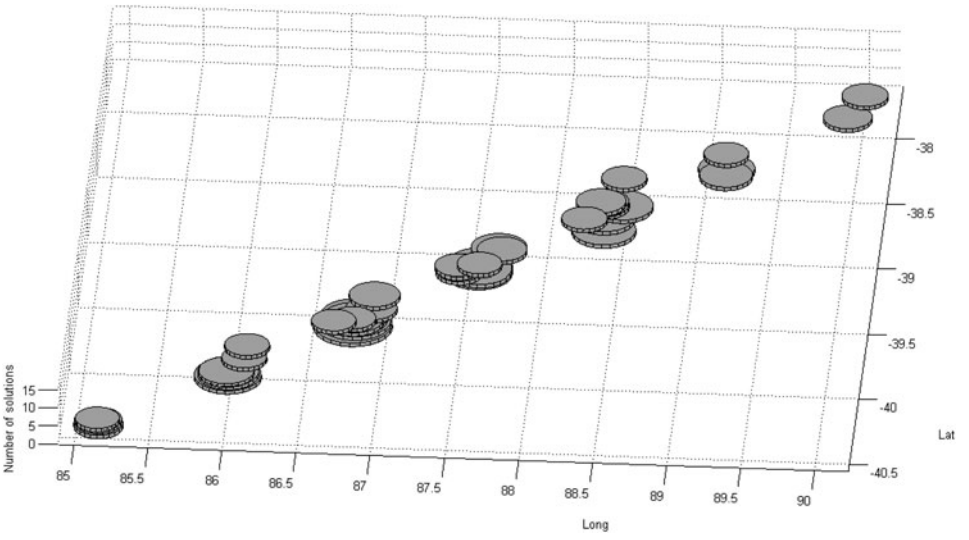

Figure 4. Position of the end of flight (E) for each of the 38 consistent solutions.

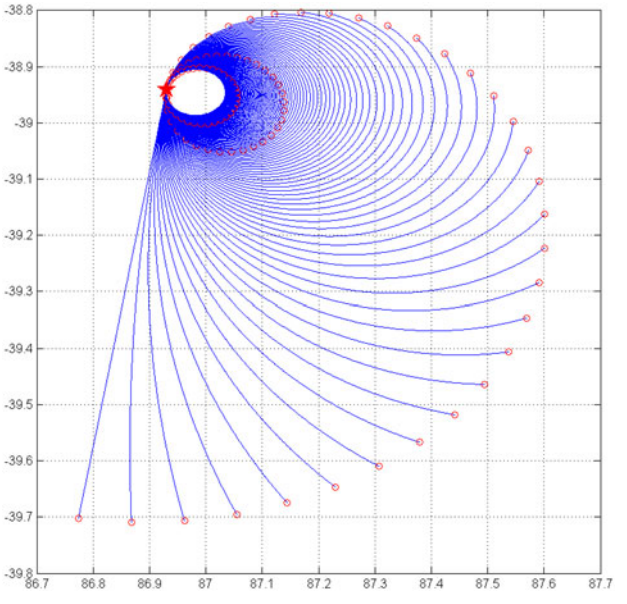

Figure 5. The locus of the end of flight positions (E^*) for solution ***11*** considering a constant angular velocity turn during glide descent; the circles represent the possible points of impact for each respective angular velocity.

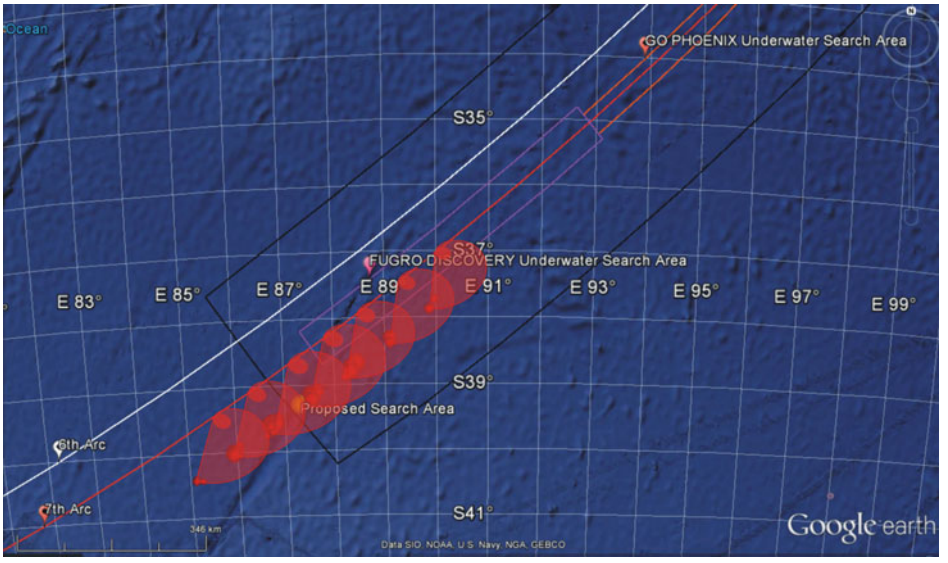

Figure 6. The end of flight point (*E*) for each of the 38 consistent solutions (discs); the weighted average of these points is represented by a light colour disc; the transparent areas resulting from the turning glide descent model (Figure 5) were positioned on the calculated end of flight points to give a probable area of impact; the ellipses on the 7th arc represent the most probable areas of impact.

the top of descent (t_{G*}) calculated with the integration of the fuel flow until the moment of fuel exhaust. The relative error ranges between −7·2% and +2·3%. For nine solutions (represented in yellow), the relative time error stays within ±1% (254 seconds of flight in absolute value), which is remarkable, given the inherent uncertainty caused by the manoeuvres before the last turn. Moreover, these small relative errors are symmetrically distributed in the range of the consistent solutions. Such a distribution appears to validate the results of the optimisation. The relative time error filter discards the lower *FL* solutions, such as solutions ***3***, ***15,*** and ***32***. Also, this filter discards the lower *M* solutions, such as ***8*** and ***26***. Given the double validation, from the optimisation and the fuel burn simulation, solutions at the upper end of the *FL* and *M* scales stand out, e.g. solution ***11***.

The places where the flight might have ended in the 38 most probable scenarios are represented in Figures 4 and 5. The places seem clustered in seven isolated groups, but the gaps between these groups might be equally interesting for searching. The solution-clustering phenomenon is probably a consequence of selecting integer values for *TK*. In reality, *TK* could have very well been a rational number, in the case of the third hypothesis of the FMS programming presented above, a "DIRECT TO" a distant point given by *LAT* and *LONG*. Figure 8 illustrates the whole simulated trajectory, which corresponds to one of the solutions (***11***). The last portion of this trajectory is made visible at a better scale in the inset.

These 38 end of flight points were calculated assuming that the glide descent was flown with a constant heading (no turn). Since the probability of a turn due to the

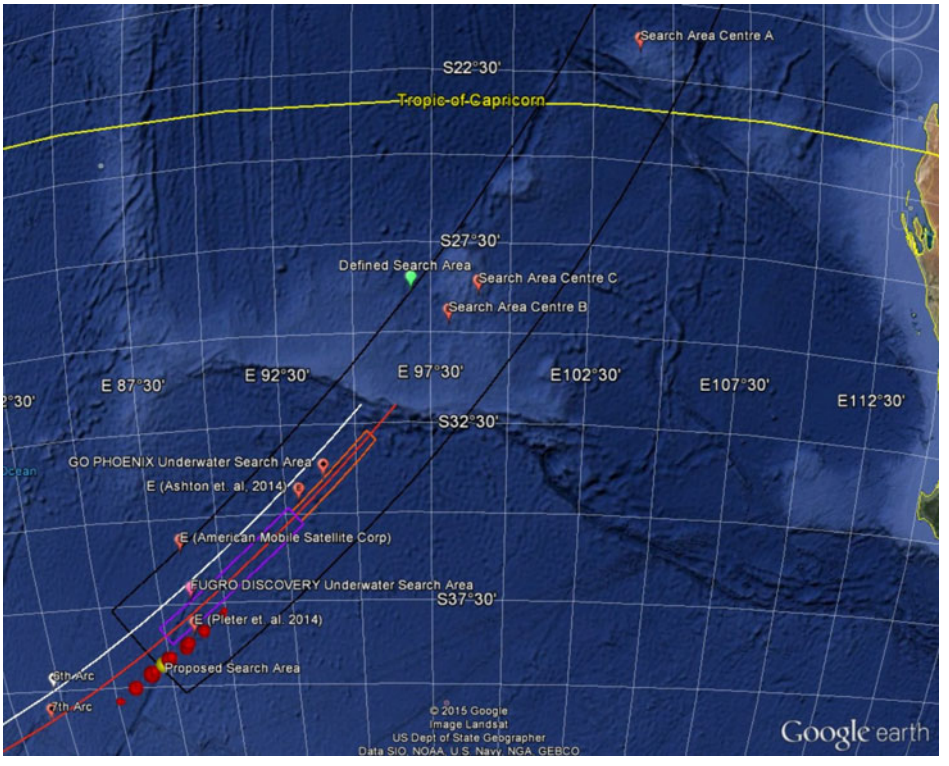

Figure 7. The end of flight point (*E*) for each of the 38 consistent solutions, compared to the current search areas and to other results published (CNN, 2014; Australian Government, 2014; Ashton et al., 2014; Pleter and Constantinescu, 2014).

initial thrust asymmetry is high (ATSB, 2014a; 2014b - MH370 - Definition of Underwater Search Areas), and the rate of turn (the angular velocity) is not known, a locus of all potential end of flight points (*E**) was developed and illustrated in Figure 5. All trajectories in Figure 5 correspond to the end of flight point of Solution ***11***, and are all turning trajectories with incremental angular velocities. The circles at the end of each same-length orthodrome trajectory represent potential points of impact with the water.

In reality, the turn could have been with variable angular velocity. The fixed angular velocity model in Figure 5 however includes in the envelope of the *E** points all possible impact points. In Figure 6, for each cluster of *E* solutions, the corresponding *E** envelope was represented as a transparent area. Out of this area, the ellipses on the seventh arch illustrate the spiral dive, which could be a higher probability impact area.

In Table 8 the same 38 solutions were placed on their *FL*s, making it obvious that the fuel burn criterion favours the higher *FL*s solutions (in yellow). Flying in a denser atmosphere, although geometrically consistent with the *BTO*s, would have fuel starved the engines much earlier than the moment t_G, which is known.

For the same solution ***11***, the simulated ground speed variation over the entire flight was represented in Figure 9. The ground speed is calculated as the vector addition

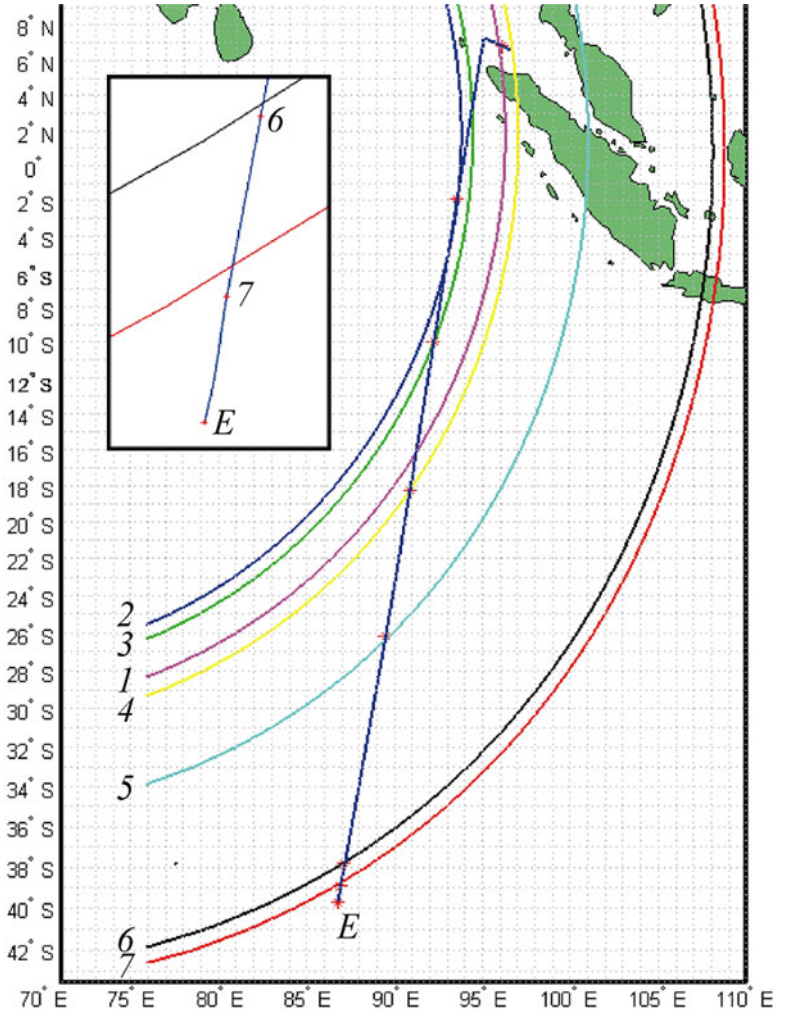

Figure 8. Quasi-circles of intersection between the satellite-centred spheres and the isobaric surface of the aircraft taken parallel to the WGS-84 rotation ellipsoid and the trajectory of MH370 as simulated for solution ***11***. Inset illustrates final segment with a slight drift both ways to the effect of the crosswind on the glide descent trajectory.

between the horizontal component of the true airspeed and the local wind velocity. For a possible validation of such a trajectory with a method based on *BFO*, Table 9 indicates the ground speed in the seven moments of the seven pings, decomposed in the ECEF framework.

The inclusion of the wind vector field in simulating the flight increased the relevance, as shown in Table 7. The inconsistency of the best-fit trajectories is between 6 and 15 times worse in cases where the wind vector field is not used. This validates the simulation and the use of the proper wind vector field, which is one of the few certain facts regarding this flight.

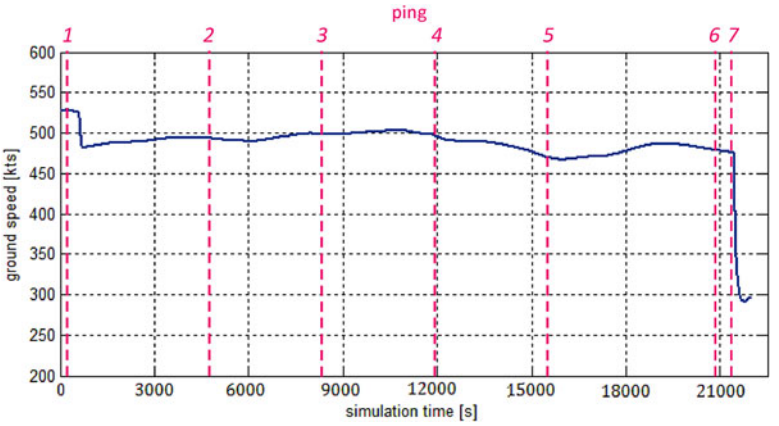

Figure 9. Simulated MH370 ground speed variation (solution ***11***).

Table 9. Solution **11** ground speed decomposed in ECEF reference for the seven quasi-circles.

ECEF	1	2	3	4	5	6	7
x′(m/s)	246·10194	41·08357	42·09721	41·21286	39·08501	33·95766	33·19933
y′ (m/s)	12·56416	−5·61979	−42·02263	−77·77739	−104·78226	−150·01248	−152·87285
z′ (m/s)	113·88568	−248·75327	−248·00685	−238·06273	−212·53179	−190·78845	−186·75045
t (s)	210	4743	8346	11967	15564	20940	21450
gs (kts)	528·3	493·4	498·9	496·3	469·3	478·3	475·4

7. CONCLUSIONS. The method presented uses the ranges determined by the last six pings along the unknown portion of the cruise flight, avoiding calculations based on the carrier frequency drift. Thus, an issue of geometric ill conditioning of the problem is avoided (since the relative aircraft-satellite speed vector is almost perpendicular to the aircraft ground speed vector). In a multimodal optimisation loop with complete search, the flight is simulated based on a dynamic model, determining the unknowns of the flight, which best fit the known facts. Thus, the method gives simultaneously the time from the last known position until the left turn, the track, and the Mach number of the cruise. The flight level can be used as a parameter of the optimisation.

All the 38 solutions found have a flight ending point *E* falling closely to each other, as illustrated in Figures 4, 6, and 7. The search area proposed by this paper may be approximated as a rectangle aligned with the 7th arch, with the following corners: S39°46′35″ E84°35′51″; S40°43′18″ E85°24′09″; S37°38′09″ E91°09′40″; S36°47′14″ E90°12′56″.

Figures 6 and 7 illustrate the most probable end of flight points calculated in this paper, in contrast to other published results (Ashton et al., 2014; Hradecky, 2014; CNN, 2014; Australian Government, 2014; Pleter and Constantinescu, 2014).

ACKNOWLEDGEMENTS

The authors wish to express their gratitude to the following contributors to their work: the reviewers of the Journal of Navigation, Capt. B787-B777 Dumitru Oprisiu, B777 Licensed Aircraft Engineer Adrian Matei, and Simon Hradecky (www.avherald.com).

REFERENCES

Ashton, C., Schuster-Bruce, A., Colledge, G. and Dickinson, M. (2014). The Search for MH370. *The Journal of Navigation*, **68**(1), 1–22.

ATSB. (2014a). Australian Transport Safety Bureau, MH370 - Definition of Underwater Search Areas - 26 June 2014, Accessed 6 October 2014.http://atsb.gov.au/media/5243942/ae-2014-054_mh370_-_definition_of_underwater_search_areas_18aug2014.pdf

ATSB. (2014b). Australian Transport Safety Bureau, MH370 – Flight Path Analysis Update - 8 October 2014. http://atsb.gov.au/media/5163181/AE-2014-054_MH370%20-flightPathAnalysisUpdate.pdf Accessed 22 November 2014

Australian Government. (2014). Department of Infrastructure and Regional Development. (2014). http://www.jacc.gov.au/media/maps/index.aspx Accessed 21 August 2014.

Boeing. (1992a). *Boeing 777-200/-200ER Technical Characteristics*. http://www.boeing.com/boeing/commercial/777family/pf/pf_200product.page. Accessed 1 June 2014.

Boeing. (1992b). *Boeing 777 Flight Crew Training Manual*. Boeing.

Bulfer, B. and Gifford, R. (1999). *Big Boeing FMC User's Guide*. Leading Edge Publications.

CNN. (2014). *American Mobile Satellite Corp.* http://edition.cnn.com/2014/06/18/world/asia/malaysia-missing-plane/index.html Accessed 10August2014.

Filippone, A. (2006). *Flight Software - Sensitivity Analysis on Fuel Burn B777-300ER*, The University of Manchester. http://www.flight.mace.manchester.ac.uk/aircraft-performance-software/case-studies/by-aircraft-and-route/case-study-boeing-b777.html. Accessed 5 July 2014.

Hradecky, S. (2014). *Crash: Malaysia B772 over Gulf of Thailand on Mar 8th 2014, aircraft missing, data indicate flight MH-370 ended west of Australia*. www.avherald.com. Accessed 13 August 2014.

INMARSAT. (2014). MH370 Data communication logs, Accessed 15 August 2014. http://www.dca.gov.my/mainpage/MH370%20Data%20Communication%20Logs.pdf

Khadilkar, H. (2011). Estimation of Aircraft Taxi-out Fuel Burn using Flight Data Recorder Archives, Masters Dissertation, *Massachusetts Institute of Technology*.

Malaysian Government. (2014). Office Of The Chief Inspector Of Air Accidents Ministry Of Transport Malaysia, MH 370 Preliminary Report Serial 03/2014, Accessed 11 June 2014. http://www.dca.gov.my/MH370/Preliminary%20Report.pdf

NOAA. (2014). *NOAA National Operational Model Archive & Distribution System*. nomads.ncdc.noaa.gov/data.php?name=access#hires_weather_dataset. Accessed 1 June 2014.

Pereira, R. L. (2011). Validation of software for the calculation of aerodynamic coefficients, Degree Project. *Linköping University*.

Pleter, O. T. and Constantinescu, C. E. (2014). Possible Trajectories of Flight Malaysian 370 (plenary presentation), INCAS, *International Conference of Aerospace Sciences "AEROSPATIAL 2014"*. Bucharest 18–19 September 2014.